Matrix mechanics regulates epithelial defence against cancer by tuning dynamic localization of filamin

Shilpa Pothapragada
TIFR Centre for Interdisciplinary Sciences
Praver Gupta
TIFR Centre for Interdisciplinary Sciences
Soumi Mukherjee
TIFR Centre for Interdisciplinary Sciences
Tamal Das (tdas@tifrh.res.in)
TIFR Centre for Interdisciplinary Sciences https://orcid.org/0000-0002-6576-5552

Article

Keywords: Mechanical microenvironment, Extracellular matrix stiffness, Epithelial defence against cancer (EDAC), Cell competition, Cytoskeletal proteins, Dynamic localization

Posted Date: October 26th, 2020

DOI: https://doi.org/10.21203/rs.3.rs-93643/v1

Version of Record: A version of this preprint was published at Nature Communications on January 11th, 2022. See the published version at https://doi.org/10.1038/s41467-021-27896-z.

Title: Matrix mechanics regulates epithelial defence against cancer by tuning dynamic localization of filamin

Short title: Matrix stiffening attenuates epithelial defence against cancer

Shilpa P. Pothapragada[1], Praver Gupta[1], Soumi Mukherjee[1], and Tamal Das[1,*]

1. TIFR Centre for Interdisciplinary Sciences, Tata Institute of Fundamental Research Hyderabad (TIFR-H), Hyderabad – 500 046, India
[*]All correspondence should be addressed to T.D., Email: tdas@tifrh.res.in

Keywords: Mechanical microenvironment, Extracellular matrix stiffness, Epithelial defence against cancer (EDAC), Cell competition, Cytoskeletal proteins, Dynamic localization

ABSTRACT

In epithelia, normal cells recognize and extrude out newly emerged transformed cells by competition. This process is the most fundamental epithelial defence against cancer, whose occasional failure promotes oncogenesis. However, little is known about what factors determine the success or failure of this defence. Here we report that mechanical stiffening of extracellular matrix attenuates the epithelial defence against activated $HRas^{V12}$-transformed cells. Using photoconversion labelling, protein tracking, and loss-of-function mutations, we attribute this attenuation to stiffening-induced perinuclear sequestration of a cytoskeletal protein, filamin. On soft matrix mimicking healthy epithelium, filamin exists as a dynamically single population, which moves to the normal cell-transformed cell interface to initiate transformed cell-extrusion. But, on stiff matrix mimicking fibrotic epithelium, filamin redistributes into two dynamically distinct populations, including a new perinuclear pool, which cannot move to the cell-cell interface. A tug-of-war between filamin-Cdc42 and filamin-perinuclear cytoskeleton interactions controls this differential filamin localization and hence, determines the success or failure of epithelial defence on soft versus stiff matrix. Together, our study reveals how pathological matrix stiffening leads to a failed epithelial defence at the initial stage of oncogenesis.

INTRODUCTION

In the micro-ecosystem of epithelial tissues, epithelial cells display an extraordinary ability of maintaining the tissue homeostasis in face of incessant sprouting of transformed cells[1-4]. In general, any newly emerged transformed cell gets actively extruded out of the tissue by the surrounding normal cells[2,3,5-8]. This process is the most fundamental immune system-independent epithelial defence against cancer (EDAC)[1,2,4,9-13] and belongs to a larger class of tissue quality-control processes, collectively known as cell competition[1,3]. Cell competition in general describes any process involving a struggle for space between two cell populations, in which the 'winner' population eliminates the 'loser' population in a non-cell autonomous manner. It plays critical roles in *Drosophila* wing epithelial development[2,3,14], mammalian tissue dynamics[15] during skin development[16], and tumour suppression in thymus[17]. EDAC, on the other hand, refers specifically to the elimination of the transformed cells that either lack a tumour suppressor protein[18] or express a constitutively active form of an oncogene such as HRAS[1,9,12,19]. Oncogene-expressing transformed cells leave the epithelial layer in form of apical extrusion or basal delamination, only if these cells are surrounded by the normal epithelial cells[9]. Importantly, occasional failure of EDAC leads to hyperplastic proliferation and cancer[1,2]. Despite some recent progress made towards uncovering the molecular players of

EDAC[9,12,19,20], the key biochemical and biophysical factors that determine whether newly emerged transformed cells get extruded from the tissue or can continue to belong there, remain largely elusive[7].

Nevertheless, it is evident that EDAC-mediated removal of transformed cells requires extensive reorganization of force-bearing cytoskeletal elements in the surrounding normal cells, particularly at the interface between normal and transformed cells[5,19,21-23]. These observations indicate possible mechanical modulations of EDAC[5,6,9,21-25]. One would then presume that EDAC might respond to the mechanical properties of the tissue microenvironment, including the extracellular matrix (ECM) stiffness, and this parameter could be a critical factor in determining the success or failure of EDAC. In fact, matrix stiffness plays a very critical role in cancer progression and metastasis at the advanced oncogenesis stage[26-29]. At this stage, cancer-associated stiffening of extracellular matrix propels the transformed cells to disrupt the mono-layered architecture of the epithelium, to proliferate without contact inhibition, and to migrate out of primary tumour[26,28]. In contrast, the role of matrix stiffness on the initial pre-malignant stage of carcinogenesis, including EDAC, remains mostly unknown. Such lack of knowledge is surprising given that one should expect the effect of matrix stiffness to be very pronounced during the initial transformation events wherein the transformed cell still bears the modulations imposed by the host tissue microenvironment. Interestingly, pathological conditions like fibrosis, hyperactive wound healing, obesity, and ageing can induce tissue stiffening, and all of these conditions correlate with high cancer risk[30,31]. However, it remains elusive whether such pre-existing fibrotic or pathologically stiffened tissue affects the success or failure of EDAC and if it indeed does that, what could be the connecting molecular mechanisms. Here, we discover matrix mechanics as a micro-environmental factor that decides the success or failure of EDAC and elucidate a new molecular mechanism by which it regulates EDAC.

RESULTS

Matrix stiffness regulates the extrusion of HRas^{V12}-transformed cells in EDAC. First, to examine whether matrix stiffness could really alter the outcome of EDAC, we used a well-established mammalian model of EDAC[9,13,32] (Figs. 1a-b) and performed EDAC experiments on ECM of varying stiffness that satisfied the range of physiological and pathological elasticity of healthy and fibrotic epithelial matrix[30,33] (Fig. 1c). The EDAC model involved normal epithelial cells competing against and eliminating transformed cells expressing a constitutively active HRas protein (HRas^{V12}) (Figs. 1a-b). A tetracycline-inducible promoter controlled HRas^{V12} expression, which enabled us to initiate the competition process when intended. We first mixed normal or wild-type epithelial cells (MDCK-WT) and cells with tetracycline-inducible GFP-tagged HRas^{V12} stably integrated in the genome (MDCK-GFP-HRas^{V12}) in 40:1 ratio (Supplementary Fig. 1a) and cultured a mosaic monolayer of these populations in absence of tetracycline. Subsequently, addition of a stable tetracycline-derivative, doxycycline, in the medium triggered HRas^{V12} expression, which became apparent at 30 minutes post-induction. HRas^{V12}-transformed cells started rounding up after three hours, and most of them extruded within eight-to-ten hours (Supplementary Fig. 1b, Supplementary Video 1, Fig. 1b). We performed this experiment on collagen I-coated hydrogel substrates of six individual discrete stiffness values, having elastic modulus of 1.2, 4, 11, 23, 35, or 90 kPa[30,33] (Fig. 1c). For each stiffness, we counted the fraction of HRas^{V12}-expressing colonies that extruded at 6 hrs post-induction (Fig. 1c, preliminary extrusion data at 4 hrs data shown in Supplementary Fig. 1c) and observed that this fraction decreased drastically on substrates stiffer than 11 kPa (Fig. 1c). We thus classified the 1.2, 4, and 11 kPa substrates as 'soft', mimicking healthy epithelium and 23, 35, and 90 kPa substrates as 'stiff', mimicking fibrotic epithelium (Fig. 1c). Interestingly, previous studies had recorded an increase in ECM stiffness from 0.1-5 kPa in healthy

epithelium to 25-100 kPa in fibrotic epithelium[34,35], which justified our classification and the transition stiffness value (> 11 kPa) that we found. What happened to the transformed cells that did not extrude on stiff substrate? These cells remained in the monolayer as long as we monitored them, up to 24 hours post-induction and eventually showed long basal protrusions and prominent basal actin fibres (Fig. 1d). These features were absent in the normal cells.

We also wondered how ECM stiffness might perturb EDAC in an organotypic 3D cyst model, which shares many features with a secretory epithelium *in vivo* and has been instrumental in understanding epithelial oncogenesis[26,36]. The wild-type MDCK cells embedded within ECM gradually formed near-spherical monolayers, each surrounding a hollow lumen (Fig. 1e). We then transfected a fraction of these cells with the tetracycline-inducible GFP-HRas^{V12} construct and initiated the transformation with doxycycline. The effect of ECM stiffness on EDAC was clearly evident in these organotypic 3D cysts (Fig. 1e). Even at eight hour post-induction with doxycycline, transformed cells continued to be a part of the epithelium in stiff ECM, while they started extruding from four-hour post-induction in soft ECM (Fig. 1e). Collectively, these results demonstrate that ECM stiffness has a decisive effect on the efficacy of EDAC-associated cell competition, where stiff ECM inhibits the elimination of transformed cells.

Differential localization of filamin on soft versus stiff matrix determines EDAC efficacy. We next looked for the molecular mechanism by which stiff ECM inhibited EDAC-induced cell extrusion. Extrusion of transformed cells requires remodelling of actin cytoskeleton in the normal cells that directly interface with the former[19,21-23]. Since ECM stiffness alters the cellular localization of many force-sensitive cytoskeleton-related proteins[37,38], we initially checked whether any actin-binding or actin-crosslinking protein showed a localization difference on soft versus stiff ECMs in normal cells (Supplementary Fig. 2). An actin filament cross-linking protein, FilaminA (FLNA, referred as filamin hereafter), emerged as the most promising candidate (Fig. 2a), considering its stiffness-sensitive perinuclear localization in normal cells (Figs. 2a-b, Supplementary Fig. 3a). On soft ECM, filamin localized to cytoplasm and to cell-cell interface, while on stiff ECM, a significant fraction of filamin molecules localized to perinuclear region (Figs. 2a-b, Supplementary Fig. 3a). Actin counter-staining and subsequent confocal microscopy (Supplementary Fig. 3b) and ultrastructure expansion microscopy (U-ExM)[39] (Fig. 2c) both revealed that perinuclear filamin molecules co-localized with perinuclear actin cytoskeleton on stiff substrate. While a previous report had reported filamin accumulation at normal cell-transformed cell interface and that depleting filamin in normal cells abrogated EDAC[19], this stiffness-sensitive perinuclear localization is a unique finding. Relevantly, on stiff ECM, filamin showed depleted interfacial localization and enhanced perinuclear localization than on soft substrate (Fig. 2b). We also observed identical pattern of filamin localization in the 3D cyst model (Fig. 2d).

Is this filamin localization pattern relevant to EDAC? In the normal cells interfacing with HRas^{V12}-expressing cells, filamin showed increased interfacial fraction (Figs. 2b and 2d), indicating that during competition filamin relocates to cell-cell interface[19]. We, therefore, hypothesized that perinuclear filamin on stiff ECM perhaps sequesters this interfacial pool and thus makes a large fraction of filamin unavailable for EDAC. To test this hypothesis, we started off by stably over-expressing filamin in normal cells to compensate for the loss of interfacial fraction on stiff ECM (Fig. 2e, *top*). The filamin over-expressing cells showed clear interfacial and perinuclear filamin pools, at the same time, on stiff ECM (Fig. 2e, *top*). We then quantified the fraction of extruded HRas^{V12}-expressing colonies during the competition between filamin-overexpressing normal cells and HRas^{V12}-expressing cells (Fig. 2e, *bottom*). Filamin overexpression indeed rescued the extrusion of transformed colonies on stiff ECM, rendering EDAC insensitive to substrate stiffness (Fig. 2e, *bottom*).

We then performed direct experiments to study the dynamics of filamin localization during EDAC on soft versus stiff ECM and to elucidate the effect of perinuclear sequestration of filamin on stiff ECM during EDAC (Fig. 2f, Supplementary Videos 2-3). To this end, we expressed moderate levels of filamin tagged with a green-to-red photoconvertible fluorescent protein, mEos2, in normal cells and selected those mEos2-filamin expressing cells that interfaced with at least one $HRas^{V12}$-expressing cell. We then photoconverted a population of mEos2-tagged filamin molecules from green to red, at a point nearly halfway between the cell-cell interface and the cell nucleus (Fig. 2f). We subsequently studied during EDAC, where those photo-converted filamin molecules localized to. On repeated cycles of photoconversion, filamin molecules invariably moved to cell-cell interface on soft ECM (Fig. 2f, *top panels*, Supplementary Video 2). On stiff ECM, however, photoconverted filamin predominantly moved to the perinuclear region (Fig. 2f, *bottom panels*, Supplementary Video 3). Moreover, a separate set of photobleaching experiments in mApple-filamin expressing cells showed that on stiff ECM, filamin had two dynamically different populations – interfacial and perinuclear (Supplementary Figs. 3c-d), in terms of the speed of recovery after photobleaching. On stiff ECM, perinuclear population was more dynamic and recovered faster than the interfacial population (Supplementary Figs. 3c-d). Interestingly, comparing soft versus stiff ECM, the dynamics of perinuclear population on stiff ECM matched very closely to that of interfacial population on soft ECM (Supplementary Fig. 3d), indicating that from the dynamics perspective, the perinuclear population of filamin on stiff ECM behaved more similarly to the interfacial population of filamin on soft ECM than to the interfacial population on stiff ECM (Supplementary Fig. 3d). Importantly, photobleaching experiments did not reveal any dynamic differentiation of filamin on soft ECM where a prominent perinuclear population was anyway missing. Collectively, guided by these photoconversion and photobleaching experiments, we propose that filamin molecules can be imagined figuratively as the balls rolling downhill to two competing attractor energy sinks, located at the cell-cell interface (*left*) and at the perinuclear region (*right*) (Fig. 2g). Both fixed-cell and dynamic experiments provided converging evidences proving that on stiff ECM, the perinuclear cytoskeleton indeed acted like a sink (Fig. 2g), which reduced the fraction of filamin molecules available for EDAC at the interface between normal and transformed cells. On stiff ECM, therefore, the interaction between normal and transformed cells fails to initiate the extrusion of transformed cells.

Cdc42 and perinuclear cytoskeleton determine differential filamin localization. We next asked what molecular signalling pathways decided the differential filamin localization on soft and stiff ECM. To this end, small RhoGTPase Cdc42 is one of strongest filamin-binding protein with a very high interaction score of 0.979 in STRING protein interaction database (https://string-db.org/). Given that RhoGTPases in general play important roles in mechanotransduction, we speculated whether Cdc42 might have different activation on soft versus stiff ECM. Transfecting the normal cells with a förster resonance energy transfer (FRET)-based Cdc42 activity sensor[40] indeed revealed stiffness-dependent differences in Cdc42 activity (Fig. 3a). Cdc42 activity at the cell-cell interface was broader (Fig. 3b, *top*) and stronger (Fig. 3b, *bottom*) on soft ECM than on stiff ECM. As an alternative representation for Cdc42 activity, staining for a Cdc42-activating guanine nucleotide exchange factor (GEF), Tuba[41], also indicated higher interfacial Cdc42 activation (Fig. 3c). Localization of Tuba to cell-cell interface was clearly more prominent on soft ECM than on stiff ECM (Fig. 3c). We then asked whether the interfacial localization of filamin on soft ECM might be a consequence of interfacial activation of Cdc42. To this end, we treated the normal cells cultured on soft ECM with a Cdc42-activity inhibitor, ML141, and studied the localisation of filamin upon this inhibitor treatment (Fig. 3d). This experiment revealed that upon ML141 treatment, the interfacial localization of filamin vanished while a faint perinuclear filamin ring appeared even on soft ECM (Figs. 3d-e). Interestingly, we could also induce interfacial localisation on stiff

ECM doing the reverse manipulation, where we expressed a constitutively active $Cdc42^{Q61L}$ in some cells (Fig. 3f). As compared to surrounding non-transfected cells, $Cdc42^{Q61L}$-expressing cells showed enhanced interfacial localization of filamin, on both soft and stiff ECM. Also, the stiff ECM-specific perinuclear filamin ring disappeared in $Cdc42^{Q61L}$-expressing cells (Fig. 3f, *left*). In contrast, $Cdc42^{Q61L}$ itself showed prominent interfacial as well as perinuclear localization on stiff ECM (Fig. 3f, *middle*). Hence, taken together, these experiments proved that Cdc42 activation drives the interfacial localization of filamin, especially on soft ECM. However, given that filamin and $Cdc42^{Q61L}$ did not co-localize at the perinuclear region (Fig. 3f, *right*), they indicated that Cdc42 might not be directly responsible for the perinuclear localization of filamin on stiff ECM.

We then asked what recruits filamin to the perinuclear cytoskeleton on stiff ECM. In non-epithelial cells, a refilin family protein, FAM101B or refilinB, stabilizes perinuclear actin networks by associating with filamin[42] (Fig. 4a, *top*). Does FAM101B recruit filamin to perinuclear cytoskeleton on stiff ECM? As a preliminary evidence, we indeed found that while on soft ECM, FAM101B distributed all over the cytoplasm (Supplementary Fig. 4a). But on stiff ECM, it co-localized with filamin predominantly in the perinuclear region (Supplementary Fig. 4a). To test whether filamin-FAM101B interaction might be responsible for the perinuclear localization of filamin, we generated a mutant filamin, FLNA-[19-22] or dnFLNA, that carried only four filamin repeats. dnFLNA had been known to have a dominant negative effect on the interaction between endogenous filamin and FAM101B[42]. Expressing dnFLNA in normal cells indeed decreased the perinuclear localization of endogenous filamin and increased its interfacial pool (Figs. 4b and 4f). We moreover generated a dominant negative FAM101B (dnFAM101B) mutant[42] that lacked the one of the filamin-binding domains, BD2. This mutant also decreased the perinuclear localization of filamin and increased its interfacial pool (Figs. 4c and 4f). Together, these experiments indicated that filamin-FAM101B interaction plays a crucial role in filamin localization to the perinuclear actin cytoskeleton. Interestingly, perinuclear actin cytoskeleton is connected to the nuclear lamina via the LINC (linker of nucleoskeleton and cytoskeleton) complex, and this linkage enables direct transmission of extracellular cues such as matrix mechanics to the nuclear force-sensing machinery[43-45] (Fig. 4a, *bottom*). In fact, using a FRET-based molecular tension sensor module[46], inserted in the middle of a LINC complex protein, Nesprin1, we measured lower a FRET efficiency (Supplementary Fig. 4b). This result implied higher LINC complex tension, on stiff ECM than on soft ECM (Supplementary Fig. 4b). We, therefore, asked whether cytoskeleton-nucleoskeleton mechanical linkage could additionally be a critical factor in stiffness-sensitive perinuclear localization of filamin (Supplementary Fig. 4). To this end, we first delinked the perinuclear cytoskeleton from nuclear lamina by disrupting the LINC complex with a dominant negative Nesprin1 (dnNesprin1 or Nesprin1-KASH) lacking the cytoskeleton binding domain[44]. In another set of experiments, we disrupted the nucleoskeleton with a LaminB1 mutant (dnLaminB1or XLaminB1Δ2+)[47] that disassembled the nuclear lamina. Consequently, normal cells expressing dnNesprin1 or dnLaminB1 (Figs. 4d and 4e) showed decreased perinuclear localization of endogenous filamin (Fig. 4f), indicating that in addition to and perhaps upstream of FAM101B, perinuclear cytoskeleton-nucleoskeleton mechanical linkage was indeed a critical factor for the perinuclear localisation of filamin.

Taken altogether, these experiments involving manipulation of Cdc42 activity vis-a-vis inhibition of FAM101B-filamin interaction or disruption of LINC complex provided the molecular basis of the interfacial and perinuclear sinks, which emerged from the dynamical study earlier (Fig. 2g). They further implied that there could be a delicate competition - a tug-of-war - between filamin-Cdc42 interaction and filamin-perinuclear cytoskeleton interaction (Fig. 4g), which gave rise to these sinks. We propose that this tug-of-war, in turn, defines the differential localization of filamin. In this tug-of-war model, filamin-Cdc42 interaction 'pulls' filamin molecules towards the cell-cell interface and is stronger on soft ECM than on stiff ECM

(Fig. 4g). In contrast, filamin-perinuclear cytoskeleton interaction pulls them towards the perinuclear region and is stronger on stiff ECM than on soft ECM (Fig. 4g).

Rescuing EDAC on stiff ECM. Having identified the molecular signalling pathway that favours filamin localization to perinuclear cytoskeleton on stiff ECM, we finally wondered whether perturbing this localization would restore EDAC on stiff ECM. To this end we generated modified normal cells stably expressing the mutants that abolished perinuclear localization of filamin and increased interfacial filamin on stiff ECM (Figs. 4b-e, Supplementary Fig. 4c), including dnFLNA, dnFAM101B, dnNesprin1 or dnLaminB1. We then tested whether these cells with increased interfacial filamin could extrude the transformed cells on stiff ECM, when the former surrounded the later (Fig. 5a). Under this experimental condition, we indeed observed significantly increased extrusion of transformed on stiff ECM (Figs. 5b-e). For example, stable dnFLNA expression in normal cells surrounding the $HRas^{V12}$-expressing colonies indeed rescued the extrusion of $HRas^{V12}$-transformed colonies on stiff ECM (Fig. 5b). Similarly, normal cells stably expressing dnFAM101B were able to extrude $HRas^{V12}$-expressing colonies with equal efficacy, irrespective of substrate stiffness (Fig. 5c). Finally, stably expressing either dnNesprin1 or dnLaminB1 in normal cells also rescued the extrusion of transformed cells on stiff substrate (Figs. 5d and 5e, respectively). Hence, all four mutants that reduced the perinuclear localization of filamin (Figs. 4b-e), either by disrupting filamin-FAM101B interaction (dnFLNA and dnFAM101B) or by disrupting the nuclear mechanotransduction (dnNesprin1 and dnLaminB1) also made cell competition more or less insensitive to ECM stiffness (Figs. 5b-e). However, we also noticed some crucial quantitative differences in how these mutants affected the perinuclear filamin localization (Figs. 4b-e) and rescued EDAC on stiff ECM (Figs. 5b-e). Firstly, on transient transfection, some normal cells expressing less-than-optimal levels of either dnFLNA or dnFAM101B still showed finite perinuclear filamin localization on stiff ECM (Figs. 4b-c, cells marked by green arrows). In contrast, perinuclear filamin was distinctly absent in any cells that expressed detectable levels of either dnNesprin1 or dnLaminB1, irrespective of the expression heterogeneity (Figs. 4d-e). These two contrasting sets of results indicated that the integrity of cytoskeleton-nucleoskeleton mechanical linkage could be upstream of the FAM101B-mediated filamin localization. Any loss of its integrity, therefore, has more prominent effect on filamin localization than what disrupting FAM101B-Filamin interaction has on the same. This conclusion is further corroborated by the differential extent of EDAC rescue on stiff ECM (Figs. 5b-e), where the degree of rescue by either dnNesprin1 or dnLaminB1 was more pronounced than by either dnFLNA or dnFAM101B. Nevertheless, in spite of these subtle differences, collectively, these experiments established the perinuclear localization of filamin on stiff ECM to be a clear molecular cause behind the failure of EDAC on stiff ECM and suggested possible therapeutic targets in future. Taken all experimental results together, here, we not only discovered and established matrix mechanics as a crucial micro-environmental factor that decided the success or failure of EDAC, but also elucidated a new molecular mechanism by which matrix mechanics regulated EDAC, thus integrating processes occurring across several length-scales (Fig. 5f).

DISCUSSION

Over the years, various studies have either implied or demonstrated that the mechanical forces could be a crucial factor in all stages of EDAC and cell competition, including cell-cell sensing, cellular reorganization, and cell extrusion[1,5,6,21,24,25]. These studies have further shown that given a specific tissue- and mutation-context, mechanical forces can have either indirect or direct effect on cell competition[5]. For example, forces can indirectly influence the elimination of transformed cells by modulating the cell shape and the geometry of cell-cell interface[21].

Alternatively, they can directly induce transformed cell extrusion by compressing the 'loser' cells and triggering their apoptosis[24]. Nevertheless, given that in the epithelial tissue, cell-cell and cell-matrix forces are tightly regulated, the role of mechanical forces on EDAC could be a simple extrapolation of the epithelial homeostasis of cell density and the constraints imposed by the epithelial architecture[29,36]. To this end, while previous works have elucidated a dynamic modulation of cell-cell junctions during cell competition[21-23], the precise role of cell-matrix interaction has remained elusive. Specifically, what has remained mostly speculative is the role of tumour microenvironment[1] and the mechanical cues coming from it on the strength and the outcome of EDAC. To this end, looking for the microenvironmental factors that might decide the success and failure of EDAC, our study reveals that an abnormally stiffened ECM prevents the EDAC-mediated elimination of $HRas^{V12}$-transformed cells from both epithelial monolayer and 3D epithelial cyst system (Figs. 1a and 1e). The ECM stiffness, thus, emerges to be a critical mechanical parameter of the tumour microenvironment regulating the most basic immune system-independent epithelial defence against cancer (Fig. 5f).

Relevantly, over the last two decades, it has also emerged that mechanical cues originating from extracellular matrix play a decisive role in the cellular fate, form, and function during stem cell differentiation and organogenesis[27,33,37,45,48,49]. We also know that the synergistic integration of biochemical and mechanical signalling influenced by tissue stiffening supports the metastatic progression of a developed tumour[5,27,28]. For example, in the well-studied case of breast cancer progression, matrix stiffening by excessive collagen cross-linking disrupts the normal acinar structures of the mammary epithelium and promotes invasive phenotype with prominent protrusions, at the advanced oncogenic stage[26,27]. In contrast, through our study, we now step into previously unexplored turfs of how an existing abnormally stiffened microenvironment might dysregulate the epithelial defence against cancer, at the initial pre-malignant stage of carcinogenesis.

While our findings have several major implications for EDAC and cancer prevention, nevertheless, it remains to be explored how generally this stiffness-sensitivity applies to other EDAC-related mutations, including those in SRC kinase[50] and transcriptional coactivator YAP[51,52]. It will be also interesting to ask whether the stiffness sensitivity itself might be tissue-specific *in vivo*. While performing controlled manipulation of ECM stiffness *in vivo* could be challenging, the possible methods might include altering the tissue-specific expression level of extracellular matrix components such as perlecan or matrix cross-linking enzymes such as lysyl oxidase (LOX) [30,53]. In this work, we have, however, preferred to focus on the molecular mechanism of stiffness-mediated attenuation of EDAC and gradually gone down in the scale – from multicellular phenomenon to protein localization dynamics – to obtain an integrative view (Fig. 5f). Exploring the tissue-specificity *in vivo* is thus beyond the scope of this study.

Further, related to the origin of stiffened ECM, one may ask: What kind of events may lead to abnormal ECM stiffening? To this end, we note that fibrosis, hyperactive wound healing, chronic inflammation, ageing, and obesity have one common physiological feature – the unusual stiffening of tissue matrix, although the root cause of stiffening could be different in each case[30,31]. Interestingly, all of these pathological conditions also correlate with an elevated risk of cancer. It is, therefore, tempting to speculate that since EDAC mechanism for eliminating the mutation-harbouring cells fails on the pathologically stiffened ECM, these pre-malignant cells are likely to stay in the tissue, acquire more mutations, and ultimately develop into an aggressive tumour over the time. In fact, in a mouse model, high fat diet-induced obesity suppresses the EDAC-mediated apical elimination of $HRas^{V12}$-transformed cells from the intestinal and pancreatic epithelia[54]. Researchers found that this suppression involved both lipid metabolism and chronic inflammation. While they speculated that soluble factors secreted from immune and fibroblast cells might be affecting the competitive interaction between normal and transformed epithelial cells, the underlying molecular mechanism remains unknown[54]. Could inflammation-induced ECM stiffness be another key player here? Given that increased

production of reactive oxygen species (ROS) during inflammation can cross-link and stiffen the extracellular matrix, further investigations may give an affirmative answer to the previous question. In addition, a separate study has shown that changes in matrix stiffness correlate with changes in lipid metabolism[55], further supporting this speculation.

Next, our experiments looking for the underlying molecular mechanism led us to the dynamic and differential localization of an actin crosslinker protein, filamin, on soft versus stiff matrix. Although it is known that ECM stiffening increases the nuclear localisation of transcription factors and coactivators like YAP/TAZ, MRTF-A, NF-κB, FHL2, and TWIST1, the stiffness-sensitive perinuclear localisation of filamin is a unique observation[37,45,56]. We found that while prominent interfacial activation of Cdc42 localizes filamin to cell-cell interface on soft ECM, perinuclear actin cytoskeleton and its associated protein, FAM101B, sequesters filamin to perinuclear region, on stiff ECM. We were further able to vividly demonstrate the bias of filamin localisation through the fluorescent photo-conversion experiments (Fig. 2f). Considering the distinct movements of photoconverted filamin molecules on soft versus stiff ECM, we propose that the dynamic and differential localization of filamin on soft and stiff ECM can be depicted as a ball rolling downhill to to two competing attractor energy sinks, located at the cell-cell interface (left minimum) and at the perinuclear region (right minimum) (Fig. 4g). Consequently, a tug-of-war between the forces pulling them towards the interfacial or perinuclear minimum governs their ultimate localization (Fig. 4g). While molecular signalling associated with soft ECM pulls filamin molecules towards the cell-cell interface, that associated with stiff ECM pulls them towards the perinuclear region (Fig. 4g).

What could be further upstream of Cdc42-filamin interaction of soft ECM and perinuclear cytoskeleton-filamin interaction on stiff ECM? On Cdc42-filamin interaction part, we speculate that the enhanced interfacial activation of Cdc42 on soft ECM could be downstream of the prevalent cytoplasmic localization of YAP/TAZ[57] on soft ECM. On perinuclear cytoskeleton-filamin interaction part, however, we provide evidences that the nuclear-mechanosensing of ECM stiffness through the nucleoskeleton-cytoskeleton linkage perhaps provides the higher level control of perinuclear localisation of filamin (Figs. 4d-e). Here, it is additionally relevant to note a previous study that has shown that the application of external force assembles the perinuclear actin in a unique Ca^{2+}- and INF2 formin-dependent manner[58]. Interestingly, a recent study has found that calcium wave explosively propagating from extruding transformed cells into the surrounding normal cells leads to actin reorganization in an INF2-dependent pathway[32]. Considering these results, it will be interesting in future to see how calcium wave interacts with the filamin-dependent pathway during EDAC. In this regard, while we have focussed on the stiffness-mediated molecular changes in the normal cells, it remains an open question whether $HRas^{V12}$-expressing cells can also show similar stiffness-dependent phenotype, and whether such phenotype would have any consequences on the likelihood of these cells getting eliminated.

Finally, going back to the original question of what microenvironmental factors might decide the success and failure of EDAC, we propose that the molecular mechanism that we elucidated here, offers therapeutic targets to prevent that. Several molecules capable of softening the tissue matrix are already in clinical trial for arresting the metastatic progression[27]. We now propose that these molecules can perhaps be used for cancer prevention as well. In addition, disruption of force transmission at various levels, from cell-matrix adhesions to LINC complex, may offer other therapeutic schemes to reduce the risk of cancer. Altogether, beyond the conventional cancer cure, this study opens up a new possibility of applying mechanomedicinal strategies to cancer prevention and intends to tip the balance in favour of a successful epithelial defence against cancer.

MATERIALS AND METHODS

Cell culture. Madin-Darby canine kidney (MDCK) epithelial cell lines were used in this study. Tetracycline-resistant Wild-type MDCK (MDCK-WT) and $HRas^{V12}$-expressing MDCK (MDCK-GFP-$HRas^{V12}$) cell lines were a gift from Yasuyuki Fujita and were generated as described previously[9]. Cells were cultured in Dulbecco's modified Eagle's medium supplemented with GlutaMax (Gibco) with 10% fetal bovine serum (tetracycline-free FBS, Takara Bio) and 10 U ml^{-1} penicillin and 10 μg ml^{-1} streptomycin (Pen-Strep, Invitrogen) in an incubator maintained at 37°C and 5% CO2, unless mentioned otherwise. For setting up cell competition in monolayer, a mosaic monolayer constituting normal MDCK cells (MDCK-WT) and transformed cells (MDCK-GFP-$HRas^{V12}$) were cultured overnight in a specific ratio (40:1) on collagen-coated polyacrylamide (PAA) gels of varying stiffness in the absence of tetracycline (Supplementary Fig. 1a). Cell competition was induced after the monolayer was confluent. Specifically, GFP-$HRas^{V12}$ expression was induced by adding 5 μg ml^{-1} doxycycline (a tetracycline-derived) to the medium.

To create 3D MDCK cysts, MDCK-WT cells were cultured on TrueGel3D hydrogel following the published manufacturer's protocol (Sigma-Aldrich). A modified version of the published work was followed to obtain a substrate of known lower (1 kPa) and higher (4-9 kPa) stiffness[59]. 10^4 MDCK-WT cells were seeded onto these gels and grown in reduced Matrigel (reconstituted basement membrane, Sigma) media. Media was replaced every 2-3 days until mature cysts with clear lumen were observed post 8 days of incubation. Mature cysts were transfected with GFP-$HRas^{V12}$ plasmid using Xfect transfection reagent (Takara Bio) following the manufacturer's protocol. Transfected samples were induced by addition of 5 μg ml^{-1} doxycycline to the culture medium.

To establish stable cell lines expressing mutant proteins for rescuing EDAC on stiff ECM (Fig. 5), MDCK cells were transfected with respective plasmid DNA using Lipofectamine 2000 (Invitrogen). Selection was done in medium (DMEM-GlutaMAX) containing 400 μg ml^{-1} geneticin (Invitrogen) and stably expressing fluorescent clones were picked using cloning cylinders (Sigma). Subsequently, maintenance and passaging of stable cell lines was done in medium containing 100 μg ml^{-1} geneticin. Transient transfection with plasmids was done using Lipofectamine 2000 (Invitrogen) following the manufacturer's protocol. Post 8-12 hours of transfection, cells were trypsinized and seeded onto hydrogel substrates and cultured overnight. Upon confluent monolayer generation, cells were either fixed and immuno-stained or imaged directly.

Hydrogel preparation for compliant ECM and for traction force microscopy. To provide the cells with the compliant ECM having different stiffness, polyacrylamide hydrogels coated with collagen-I were generated and characterized as described previously[33,60]. 4% (3-Aminopropyl)triethoxysilane (APTES)-treated and 2% glutaraldehyde-activated glass bottom dishes (Ibidi) were used to cast thin polyacrylamide (PAA) hydrogel substrates. Hyrdrogel substrates of varying stiffness with elastic modulus of 1.2, 4, 11, 23, 35, and 90 kPa were prepared by mixing desired volume of 40% acrylamide and 2% bis-acrylamide as given in Supplementary Table 1. Gel surfaces were functionalized with sulphosuccinimidyl-6-(4′-azido-2′-nitrophenylamino) hexanoate (Sulfo-SANPAH, Thermo Scientific) and covalently coated with 300 μg ml^{-1} collagen-I (Invitrogen) overnight at 4℃ to ensure cell attachment. Cells were seeded onto the gel area and grown until a confluent monolayer was obtained. Cell competition studies were then carried out.

Antibodies and plasmids. Source and dilution information for all primary and secondary antibodies used in immunofluorescence staining are given in Supplementary Table 2. Details of plasmids used in this study is listed in Supplementary Table 3 with their source.

Immunofluorescence. Cells were first fixed with 4% formaldehyde diluted in 1x phosphate-buffered saline (PBS, pH 7.4) at room temperature (RT) for 15 min. Following this, cells were washed thrice with 1x PBS. To permeabilize the cells, they were treated with 0.25% (v/v) Triton X-100 (Sigma) in PBS for 10 min at RT followed by washing thrice with PBS to remove the detergent. Non-specific antibody binding was blocked by incubating the samples with 2% BSA in PBST (0.1% v/v Triton X-100 in 1x PBS) at RT for 45 minutes. Post this incubation time, blocking buffer was replaced with the primary antibody diluted in blocking buffer and samples incubated at RT for 60 minutes or at 4°C overnight. After this, samples were washed twice with PBST and thrice with PBS. Samples were then incubated at with secondary antibody tagged with fluorescent dye Alexa Fluor 594 or 647 (Invitrogen) in similar dilution as primary antibody, for 60 minutes at RT. Counterstaining cell nuclei with a DNA-binding dye 4′,6-diamidino-2-phenylindole (DAPI, 1 μg ml^{-1} in PBS, Invitrogen) and F-actin with Alexa Fluor dye conjugated phalloidin (Invitrogen) was also done at this step. Finally, samples were washed thoroughly with PBST and PBS before being imaged using confocal microscopy.

Ultrastructure expansion microscopy. The ultrastructure expansion microscopy (U-ExM) for filamin and perinuclear cytoskeleton co-localization studies was done as described previously[39], with an optimized expansion condition that retained both antibodies and fluorescent proteins. Also, in this experiment, we transfected the cells with LifeAct-GFP to visualize actin. Briefly, LifeAct-GFP MDCK cells were cultured to confluency on collagen coated 90 kPa PAA hydrogel and fixed with U-ExM fixation solution, which is 3% formaldehyde (Invitrogen) with 0.1% glutaraldehyde (Sigma) in 1X PBS. Subsequently, the samples were incubated in post-fix solution, which is 0.7% formaldehyde with 1% Acrylamide (Sigma) in 1X PBS, overnight at 37℃. Then, the samples were stained for endogenous filamin with anti-filamin antibody. Next, to enhance the retention of bound fluorophores during subsequent steps of expansion, the samples were equilibrated with the gel anchoring moiety Acryloyl-X, SE (6-((acryloyl)amino) hexanoic acid, succinimidyl ester; Thermofisher) at a concentration of 0.1 mg mL^{-1} in 1X PBS for 3 hours at room temperature. Then, the samples were immobilized in 100 μL of U-ExM monomer solution composed of 19% Sodium Acrylate (Sigma), 10% Acrylamide (Sigma), 0.1% N,N′-methylene bisacrylamide (Sigma) in 1X PBS supplemented with 0.5% ammonium persulfate (Sigma) initiator and tetramethyl ethylenediamine (Sigma) accelerator, on Parafilm in a pre-cooled humid chamber. Gelation was proceeded for 5 min on ice, and then at 37 °C in the dark for 1 hour. Samples were then transferred into ~2 ml of denaturation buffer, made of 50 mM sodium dodecyl sulfate, 200 mM NaCl, and 50 mM Tris in ultrapure water, and the pH was to adjusted to 9. The sample denaturation was allowed to proceed for 1 h at 70 °C. After denaturation, samples were placed in deionized water twice for every 30 min and then overnight at room temperature. Expanded samples were then trimmed, mounted on 35mm glass bottom dishes (Ibidi) and imaged by confocal microscopy.

Confocal microscopy. Immunostained samples were acquired using 60x water objective (UPLSAPO W, N.A=1.2, Olympus) mounted on an Olympus IX83 inverted microscope equipped with a scanning laser confocal head (Olympus FV3000). Photoconversion, photobleaching and FRET-based sensor studies were done in the same setup using a live-cell chamber supplied with humidified CO_2.

Filamin localization dynamics using photoconversion and photobleaching. Photoconversion studies were done on mosaic populations of MDCK-GFP-$HRas^{V12}$ cells co-cultured (on soft or stiff ECM) with MDCK cells that had been transiently transfected with mEos2-FilaminA-N-9. To distinguish mEos2-Filamin-expressing green normal cells from GFP-$HRas^{V12}$-expressing green transformed cells, we stained the former with CellTracker Blue

CMAC (Thermofisher), according to manufacturer protocol, before creating the mosaic monolayer. An optimally expressing mEos2-Filamin cell was chosen that interfaced with an MDCK-GFP-HRas^{V12} cell. Stimulation was done on a point region-of-interest in the mEos2-filamin cell using a 405 nm laser at 2% intensity, looped over for 25 times with a scan speed of 1000 µsec/pixel. This was immediately followed by LSM imaging of the green and red channels; 0.3% intensity, 700V PMT voltage for the green and 4% intensity, 650V PMT voltage for the red channels and filamin dynamics was subsequently tracked for 180 seconds.

Photobleaching studies were done using MDCK cells stably expressing mApple-FilaminA, cultured on soft or stiff substrate. 561 nm laser was used at 5% intensity for bleaching a region-of-interest, iterated or looped over five times with a scan speed of 200 µsec/pixel. For LSM imaging, laser power was attenuated to avoid phototoxicity. Images were collected before, immediately after, and for 60 seconds following the bleaching.

Förster resonance energy transfer (FRET)-based molecular tension and Cdc42-activity measurements. FRET experiments for Nesprin tension sensor (Nesprin-TS)[46] were carried out in the live-cell confocal setup (Olympus FV3000). MDCK cells were first plated in six-well plate (Tarsons) and transiently transfected with Nesprin-TS full length construct. After 12 hours, cells were trypsinized and cultured onto soft (4 kPa) and stiff (90 kPa) substrates overnight. Cells were then rinsed and replaced with fresh medium. Images were taken in three different channels: 1. mTFP1: 445 nm laser; filter: 460-500 nm, 2. FRET: 445 nm laser; filter: 530-630 nm, and 3. mVenus: 514 nm laser; filter: 530-630 nm. The pinhole diameter, laser intensity, and exposure times for donor, acceptor, and FRET channels were always kept constant for subsequent experiments. Each field yielded three 1024 x 1024 pixel images representing the donor, FRET, and acceptor channels. Images were then analysed using custom software written in MATLAB (MathWorks). Corrected FRET intensity was calculated by subtracting background and donor bleed-through (dbt) and acceptor cross-excitation. Here, dbt was inferred by the leak-through of mTFP1 signal into the mVenus detector. Acceptor cross-excitation was negligible. The FRET index was quantified by using the pixel-by-pixel intensity FRET (I_{FRET}) and donor (I_D) channels as: FRET Index = $cI_{FRET}/ (I_D + I_{FRET})$, where cI_{FRET} is the corrected FRET intensity = I_{FRET} - (dbt x I_D). Nesprin-headless control was also used to establish appropriate functioning activity of the Nesprin-TS full length construct.

Raichu-Cdc42 FRET based-biosensor was used for Cdc42 activity measurement in a similar manner to that of Nesprin-TS. Images were taken in three different channels: 1. ECFP: 445 nm laser; filter: 460-500 nm, 2. FRET: 445 nm laser; filter: 530-630 nm, and 3. EYFP: 514 nm laser; filter: 530-630 nm and subsequent analysis done as mentioned above.

Inhibition studies. ML141, inhibitor of the Rho family GTPase Cdc42 was obtained from Sigma. The powdered chemical form was dissolved in DMSO to make the stock. Cells cultured on soft substrate were treated with 40 µM ML141 for different time durations to inhibit Cdc42 activity.

Image analysis. To measure extrusion count, fixed samples of mosaic monolayers grown on hydrogels of varying stiffness were stained for cell nucleus with DAPI and imaged using 20x objective on Leica DMI8 inverted microscope. Rounded-up out-of-plane HRas^{V12} cell colonies were manually marked as extruded. The fraction of extruded transformed colonies over total number of transformed colonies per frame was quantified as extrusion count. Approximately 10 frames were acquired per sample (hydrogel of specific stiffness) for each independent experiment. Quantifications shown in various figures were conducted using data from three independent repeats per experiment.

To determine perinuclear and interfacial filamin, ROIs were traced out manually using selection brush tool (fixed at 10 pixel width) in FIJI (Supplementary Figs. 3a and 4d). Cell-

nuclei frame was synced with the filamin frame and used as reference for tracing perinuclear region. Interfacial regions were manually traced at the cell-cell interface. Overlapping region tracing was carefully avoided. Mean intensity values were taken for perinuclear and interfacial regions per cell. Fraction of filamin localisation per cell for each region was quantified as the ratio of the intensity of the ROI with total intensity. For quantification purpose, total intensity was the sum of the intensity of perinuclear ROI and interfacial ROI. Fluorescence images were brightness-adjusted and denoised uniformly throughout the whole image for representation purposes only. Denoising was done using PureDenoise tool in FIJI[61].

Statistical analysis. Statistical analysis was carried out in Prism (GraphPad). Statistical significance was calculated by Unpaired t-test with Welch's correction or Mann–Whitney test (two-tailed) as mentioned in the corresponding figure. Scatter-bar plots were displayed as mean ± s.e.m. In box-and-whiskers plot, centre line denotes median, box displays the interquartile range, whiskers indicate range not including outliers (1.5x interquartile range). P-values greater than 0.05 were considered to be statistically not significant. No statistical methods were used to set sample size. Quantification was done using data from at least three independent biological replicates.

AUTHOR CONTRIBUTIONS

S.P.P. and T.D. conceived the project. S.P.P., P.G., and S.M. performed experiments. S.P.P., P.G., and T.D. analysed the results. S.P.P., P.G., and T.D. wrote the manuscript. All authors agreed on the manuscript as in the submitted version.

ACKNOWLEDGEMENT

We thank G.V. Shivashankar for critical discussions and suggestions. We also thank Yasuyuki Fujita for cell lines, plasmids, and important inputs. We thank Sanjay Karki, Farah Taj, and Medhavi Vishwakarma for their technical assistance. T.D. is a DBT/Wellcome Trust India Alliance intermediate fellow and partner group leader of the Max Planck Society (MPG), Germany. Authors sincerely acknowledge generous funding from the DBT/Wellcome Trust India Alliance (grant no. IA/I/17/1/503095) as well as intramural funds at TIFR Hyderabad from the Department of Atomic Energy (DAE), Govt. of India towards supporting this project.

REFERENCES

1 Vishwakarma, M. & Piddini, E. Outcompeting cancer. *Nat Rev Cancer* **20**, 187-198, doi:10.1038/s41568-019-0231-8 (2020).

2 Moreno, E. Opinion - Is cell competition relevant to cancer? *Nat Rev Cancer* **8**, 141-147, doi:10.1038/nrc2252 (2008).

3 Vincent, J. P., Fletcher, A. G. & Baena-Lopez, L. A. Mechanisms and mechanics of cell competition in epithelia. *Nat Rev Mol Cell Biol* **14**, 581-591, doi:10.1038/nrm3639 (2013).

4 Ellis, S. J. *et al.* Distinct modes of cell competition shape mammalian tissue morphogenesis. *Nature* **569**, 497-502, doi:10.1038/s41586-019-1199-y (2019).

5 Matamoro-Vidal, A. & Levayer, R. Multiple Influences of Mechanical Forces on Cell Competition. *Curr Biol* **29**, R762-R774, doi:10.1016/j.cub.2019.06.030 (2019).

6 Bras-Pereira, C. & Moreno, E. Mechanical cell competition. *Curr Opin Cell Biol* **51**, 15-21, doi:10.1016/j.ceb.2017.10.003 (2018).

7 Merino, M. M., Levayer, R. & Moreno, E. Survival of the Fittest: Essential Roles of Cell Competition in Development, Aging, and Cancer. *Trends Cell Biol* **26**, 776-788, doi:10.1016/j.tcb.2016.05.009 (2016).
8 Wagstaff, L., Kolahgar, G. & Piddini, E. Competitive cell interactions in cancer: a cellular tug of war. *Trends Cell Biol* **23**, 160-167, doi:10.1016/j.tcb.2012.11.002 (2013).
9 Hogan, C. *et al.* Characterization of the interface between normal and transformed epithelial cells. *Nat Cell Biol* **11**, 460-U234, doi:10.1038/ncb1853 (2009).
10 Wagstaff, L., Kolahgar, G. & Piddini, E. Competitive cell interactions in cancer: a cellular tug of war. *Trends Cell Biol* **23**, 160-167, doi:10.1016/j.tcb.2012.11.002 (2013).
11 Madan, E. *et al.* Flower isoforms promote competitive growth in cancer. *Nature* **572**, 260-264, doi:10.1038/s41586-019-1429-3 (2019).
12 Kajita, M. & Fujita, Y. EDAC: Epithelial defence against cancer-cell competition between normal and transformed epithelial cells in mammals. *J Biochem* **158**, 15-23, doi:10.1093/jb/mvv050 (2015).
13 Kon, S. *et al.* Cell competition with normal epithelial cells promotes apical extrusion of transformed cells through metabolic changes. *Nat Cell Biol* **19**, 530-541, doi:10.1038/ncb3509 (2017).
14 Morata, G. & Ripoll, P. Minutes - Mutants of Drosophila Autonomously Affecting Cell-Division Rate. *Dev Biol* **42**, 211-221, doi:Doi 10.1016/0012-1606(75)90330-9 (1975).
15 Meyer, S. N. *et al.* An ancient defense system eliminates unfit cells from developing tissues during cell competition. *Science* **346**, 1258236, doi:10.1126/science.1258236 (2014).
16 Liu, N. *et al.* Stem cell competition orchestrates skin homeostasis and ageing. *Nature* **568**, 344-350, doi:10.1038/s41586-019-1085-7 (2019).
17 Martins, V. C. *et al.* Cell competition is a tumour suppressor mechanism in the thymus. *Nature* **509**, 465-+, doi:10.1038/nature13317 (2014).
18 Norman, M. *et al.* Loss of Scribble causes cell competition in mammalian cells. *J Cell Sci* **125**, 59-66, doi:10.1242/jcs.085803 (2012).
19 Kajita, M. *et al.* Filamin acts as a key regulator in epithelial defence against transformed cells. *Nat Commun* **5**, doi:ARTN 4428 10.1038/ncomms5428 (2014).
20 Ohoka, A. *et al.* EPLIN is a crucial regulator for extrusion of RasV12-transformed cells. *J Cell Sci* **128**, 781-789, doi:10.1242/jcs.163113 (2015).
21 Levayer, R., Hauert, B. & Moreno, E. Cell mixing induced by myc is required for competitive tissue invasion and destruction. *Nature* **524**, 476-+, doi:10.1038/nature14684 (2015).
22 Teo, J. L. *et al.* Caveolae Control Contractile Tension for Epithelia to Eliminate Tumor Cells. *Dev Cell* **54**, 75-+, doi:10.1016/j.devcel.2020.05.002 (2020).
23 Wu, S. K. *et al.* Cortical F-actin stabilization generates apical-lateral patterns of junctional contractility that integrate cells into epithelia. *Nat Cell Biol* **16**, 167-178, doi:10.1038/ncb2900 (2014).
24 Wagstaff, L. *et al.* Mechanical cell competition kills cells via induction of lethal p53 levels. *Nat Commun* **7**, doi:Artn 11373 10.1038/Ncomms11373 (2016).
25 Levayer, R., Dupont, C. & Moreno, E. Tissue Crowding Induces Caspase-Dependent Competition for Space. *Curr Biol* **26**, 670-677, doi:10.1016/j.cub.2015.12.072 (2016).
26 Levental, K. R. *et al.* Matrix crosslinking forces tumor progression by enhancing integrin signaling. *Cell* **139**, 891-906, doi:10.1016/j.cell.2009.10.027 (2009).
27 Mohammadi, H. & Sahai, E. Mechanisms and impact of altered tumour mechanics. *Nat Cell Biol* **20**, 766-774, doi:10.1038/s41556-018-0131-2 (2018).

28 Butcher, D. T., Alliston, T. & Weaver, V. M. A tense situation: forcing tumour progression. *Nat Rev Cancer* **9**, 108-122, doi:10.1038/nrc2544 (2009).
29 Fiore, V. F. *et al.* Mechanics of a multilayer epithelium instruct tumour architecture and function. *Nature* **585**, 433-+, doi:10.1038/s41586-020-2695-9 (2020).
30 Lampi, M. C. & Reinhart-King, C. A. Targeting extracellular matrix stiffness to attenuate disease: From molecular mechanisms to clinical trials. *Sci Transl Med* **10**, doi:10.1126/scitranslmed.aao0475 (2018).
31 Seo, B. R. *et al.* Obesity-dependent changes in interstitial ECM mechanics promote breast tumorigenesis. *Sci Transl Med* **7**, 301ra130, doi:10.1126/scitranslmed.3010467 (2015).
32 Takeuchi, Y. *et al.* Calcium Wave Promotes Cell Extrusion. *Curr Biol* **30**, 670-681 e676, doi:10.1016/j.cub.2019.11.089 (2020).
33 Engler, A. J., Sen, S., Sweeney, H. L. & Discher, D. E. Matrix elasticity directs stem cell lineage specification. *Cell* **126**, 677-689, doi:10.1016/j.cell.2006.06.044 (2006).
34 Wells, R. G. Tissue mechanics and fibrosis. *Bba-Mol Basis Dis* **1832**, 884-890, doi:10.1016/j.bbadis.2013.02.007 (2013).
35 Santos, A. & Lagares, D. Matrix Stiffness: the Conductor of Organ Fibrosis. *Curr Rheumatol Rep* **20**, doi:ARTN 2 10.1007/s11926-018-0710-z (2018).
36 Leung, C. T. & Brugge, J. S. Outgrowth of single oncogene-expressing cells from suppressive epithelial environments. *Nature* **482**, 410-U160, doi:10.1038/nature10826 (2012).
37 Dupont, S. *et al.* Role of YAP/TAZ in mechanotransduction. *Nature* **474**, 179-U212, doi:10.1038/nature10137 (2011).
38 Duan, R. *et al.* Spectrin is a mechanoresponsive protein shaping fusogenic synapse architecture during myoblast fusion. *Nat Cell Biol* **20**, doi:10.1038/s41556-018-0106 (2018).
39 Gambarotto, D. *et al.* Imaging cellular ultrastructures using expansion microscopy (U-ExM). *Nat Methods* **16**, 71-+, doi:10.1038/s41592-018-0238-1 (2019).
40 Hanna, S., Miskolci, V., Cox, D. & Hodgson, L. A New Genetically Encoded Single-Chain Biosensor for Cdc42 Based on FRET, Useful for Live-Cell Imaging. *Plos One* **9**, doi:ARTN e96469 10.1371/journal.pone.0096469 (2014).
41 Otani, T., Ichii, T., Aono, S. & Takeichi, M. Cdc42 GEF Tuba regulates the junctional configuration of simple epithelial cells. *J Cell Biol* **175**, 135-146, doi:10.1083/jcb.200605012 (2006).
42 Gay, O. *et al.* RefilinB (FAM101B) targets FilaminA to organize perinuclear actin networks and regulates nuclear shape. *P Natl Acad Sci USA* **108**, 11464-11469, doi:10.1073/pnas.1104211108 (2011).
43 Kirby, T. J. & Lammerding, J. Emerging views of the nucleus as a cellular mechanosensor. *Nat Cell Biol* **20**, 373-381, doi:10.1038/s41556-018-0038-y (2018).
44 Elosegui-Artola, A. *et al.* Force Triggers YAP Nuclear Entry by Regulating Transport across Nuclear Pores. *Cell* **171**, 1397-1410 e1314, doi:10.1016/j.cell.2017.10.008 (2017).
45 Swift, J. *et al.* Nuclear lamin-A scales with tissue stiffness and enhances matrix-directed differentiation. *Science* **341**, 1240104, doi:10.1126/science.1240104 (2013).
46 Arsenovic, P. T. & Conway, D. E. Using Nesprin Tension Sensors to Measure Force on the LINC Complex. *Methods Mol Biol* **1840**, 59-71, doi:10.1007/978-1-4939-8691-0_6 (2018).
47 Vaughan, O. A. *et al.* Both emerin and lamin C depend on lamin A for localization at the nuclear envelope. *J Cell Sci* **114**, 2577-2590 (2001).

48 Ogawa, R. & Hsu, C. K. Mechanobiological dysregulation of the epidermis and dermis in skin disorders and in degeneration. *J Cell Mol Med* **17**, 817-822, doi:10.1111/jcmm.12060 (2013).
49 Park, J. S. *et al.* Mechanical regulation of glycolysis via cytoskeleton architecture. *Nature* **578**, 621-626, doi:10.1038/s41586-020-1998-1 (2020).
50 Kajita, M. *et al.* Interaction with surrounding normal epithelial cells influences signalling pathways and behaviour of Src-transformed cells. *J Cell Sci* **123**, 171-180, doi:10.1242/jcs.057976 (2010).
51 Moya, I. M. *et al.* Peritumoral activation of the Hippo pathway effectors YAP and TAZ suppresses liver cancer in mice. *Science* **366**, 1029-1034, doi:10.1126/science.aaw9886 (2019).
52 Chiba, T. *et al.* MDCK cells expressing constitutively active Yes-associated protein (YAP) undergo apical extrusion depending on neighboring cell status. *Sci Rep-Uk* **6**, doi:ARTN 28383 10.1038/srep28383 (2016).
53 Ma, M. Q., Cao, X. Y., Dai, J. L. & Pastor-Pareja, J. C. Basement Membrane Manipulation in Drosophila Wing Discs Affects Dpp Retention but Not Growth Mechanoregulation. *Dev Cell* **42**, 97-+, doi:10.1016/j.devcel.2017.06.004 (2017).
54 Sasaki, A. *et al.* Obesity Suppresses Cell-Competition-Mediated Apical Elimination of RasV12-Transformed Cells from Epithelial Tissues. *Cell Reports* **23**, 974-982, doi:10.1016/j.celrep.2018.03.104 (2018).
55 Romani, P. *et al.* Extracellular matrix mechanical cues regulate lipid metabolism through Lipin-1 and SREBP. *Nat Cell Biol* **21**, 338-+, doi:10.1038/s41556-018-0270-5 (2019).
56 Nakazawa, N., Sathe, A. R., Shivashankar, G. V. & Sheetz, M. P. Matrix mechanics controls FHL2 movement to the nucleus to activate p21 expression. *P Natl Acad Sci USA* **113**, E6813-E6822, doi:10.1073/pnas.1608210113 (2016).
57 Sakabe, M. *et al.* YAP/TAZ-CDC42 signaling regulates vascular tip cell migration. *P Natl Acad Sci USA* **114**, 10918-10923, doi:10.1073/pnas.1704030114 (2017).
58 Shao, X. W., Li, Q. S., Mogilner, A., Bershadsky, A. D. & Shivashankar, G. V. Mechanical stimulation induces formin-dependent assembly of a perinuclear actin rim. *P Natl Acad Sci USA* **112**, E2595-E2601, doi:10.1073/pnas.1504837112 (2015).
59 Friedrich, O. *et al.* Adding dimension to cellular mechanotransduction: Advances in biomedical engineering of multiaxial cell-stretch systems and their application to cardiovascular biomechanics and mechano-signaling. *Prog Biophys Mol Biol* **130**, 170-191, doi:10.1016/j.pbiomolbio.2017.06.011 (2017).
60 Krishnan, R. *et al.* Substrate stiffening promotes endothelial monolayer disruption through enhanced physical forces. *Am J Physiol-Cell Ph* **300**, C146-C154, doi:10.1152/ajpcell.00195.2010 (2011).
61 Luisier, F., Vonesch, C., Blu, T. & Unser, M. Fast interscale wavelet denoising of Poisson-corrupted images. *Signal Processing* **90**, 415-427, doi:10.1016/j.sigpro.2009.07.009 (2010).

FIGURE LEGENDS

Figure 1. Matrix stiffening attenuates extrusion of HRas^{V12}-transformed cells during EDAC. a. Fluorescence images of GFP-HRas^{V12} expressing colony extrusion on soft (4 kPa) and stiff (90 kPa) substrates in XY-plane; followed by an illustration depicting the visual metric employed to quantify extrusion. Rounded-up cells expressing GFP-HRas^{V12} (as seen on soft ECM) are taken as extruded. Non-extruded GFP-HRas^{V12} cells remain in plane with other cells, as evident on stiff ECM. (*Bottom panels*) The yellow-dotted lines visually guide epithelium surface in XZ-plane. GFP-HRas^{V12} cells extruded over this surface on soft ECM (*left*) whereas

they remained within this surface on stiff ECM (*right*). White arrowheads indicate GFP-HRas^{V12} cells. **b.** Diagram representating different phases of extrusion of transformed cells and stiffness-dependent outcome of EDAC. **c.** Scatter bar plot depicting the fraction of GFP-HRas^{V12} expressing colonies extruded over substrates of varying stiffness at 6 hpi. Distinct decrease in extrusion of transformed cells observed with increase in substrate stiffness. The number of colonies counted is indicated inside each bar. Data are mean±s.e.m. collected over 3 independent biological replicates. Statistical significance was assessed using Mann-Whitney t-test (two-tailed). **d**. Cytoskeletal morphology of non-extruded colonies over stiff ECM at 24 hpi. White arrowheads indicate basal actin fibres associated with HRas^{V12}- cells on stiff ECM (90 kPa), stained with AlexaFluor647-Phalloidin. Inset: Magnified view of yellow-boxed region with actin fibres pointed out by white arrowheads. **e.** Immunofluorescence images of 3D cyst model for EDAC on soft and stiff ECM. Yellow arrowheads indicate the transformed cells. hpi: hours post-induction with doxycycline. **a,d,e** Scale bars: 10 μm.

Figure 2. ECM stiffness-dependent localization of filamin determines EDAC efficacy. a. Immunostaining images of mosaic monolayer of MDCK-WT:MDCK-GFP-HRas^{V12} cultured on soft (*top panels*) and stiff (*bottom panels*) ECM. From *left* to *right*: GFP-HRas^{V12}, filamin in the mosaic monolayer and magnified view of the boxed regions. Cyan arrowheads indicate interfacial filamin enrichment on soft ECM, and tellow arrowheads indicate perinuclear filamin localization on stiff ECM. Scale bars: 10 μm. **b.** Box-and-whiskers plot depicting the fraction of filamin mean fluorescence intensity at perinuclear and interfacial regions, per cell, on soft (4 kPa) and stiff (90 kPa) ECM. Statistical significance was assessed using unpaired student t-test with Welch's correction (two-tailed). **c.** Ultrastructure expansion microscopy (U-ExM) for MDCK-LifeAct cells immunostained for filamin show distinct perinuclear co-localization (black arrowhead, bottom magnified panels). Scale bar: 1 μm (*top*) and 2 μm (*bottom*). **d.** Immunofluorescence images of filamin immunostaining in 3d cysts on soft (*left*) and stiff ECM (*right*) followed by the magnified view of boxed region. Presence or absence of filamin perinuclear localization indicated by yellow arrowheads for soft (absence) and stiff (presence) within MDCK-WT cells surrounding MDCK-GFP-HRas^{V12} cells. **e.** Fluorescence images of mosaic monolayer of filamin-over expressing MDCK cells and MDCK-GFP-HRas^{V12} co-cultured on stiff substrate with magnified view of the boxed region. Yellow and cyan arrowheads indicate perinuclear and interfacial filamin accumulation respectively. (*Bottom*) Scatter bar plot depicting the fraction of GFP-HRas^{V12} expressing colonies extruded over substrates of varying stiffness. For each stiffness, left bars are for mock MDCK-WT:MDCK-GFP-HRas^{V12} and right bars are for MDCK-mApple-FLNA:MDCK-GFP-HRas^{V12} mosaic populations. Stable over-expression of filamin in surrounding cells rescued extrusion of transformed populations on stiff substrate. **f.** Photoconversion of mEos2-filamin to study filamin localization dynamics. mEos2-filamin cell interfacing with an HRas^{V12} cell was stimulated and tracked for 180 seconds, as depicted in the schematic. Snapshots of mEos2-filamin dynamics indicating dynamic changes in localization. Kymographs of interfacial (i, green box) or perinuclear (ii, white box) regions show enrichment of filamin at interface (soft ECM, *top panel*) or perinuclear region (stiff ECM, *bottom panel*). Scale bars: 5 μm. **g.** Filamin attracting sinks. Filamin molecules can be imagined as the balls rolling downhill in the energy landscape to two competing attractor energy sinks, located at the cell-cell interface (*left*) and at the perinuclear region (*right*). On soft ECM, interfacial sink is deeper than perinuclear sink. Therefore, it attracts more filamin molecules than towards perinuclear. The scenario reverses on stiff ECM.

Figure 3. Interaction with Cdc42 determines interfacial filamin localization. a. Raichu-Cdc42 FRET biosensor expressed in MDCK-WT cells cultured on soft (*top*) and stiff (*bottom*) ECM. **b.** (*Top*) Line scan of normalized gray values from the FRET channel (white double-

arrowed line in (**a**) from cells cultured on both soft and stiff ECM indicate higher FRET values at cell-cell interface on soft ECM. (*Bottom*) Box-and-whiskers plot of mean FRET index from soft and stiff ECM shows significant reduction in cells cultured on stiff ECM, indicative of higher Cdc42 activity on soft ECM. **c.** Immunofluorescence images of MDCK-WT cells co-stained for filamin and Tuba (Cdc42-GEF). Yellow arrowhead indicates enrichment of Cdc42-GEF at interfacial region on soft ECM (top) and at perinuclear region on stiff ECM (bottom). **d.** Immunofluorescence images of MDCK-WT cells cultured on soft ECM treated with Cdc42 inhibitor, control DMSO (*top*) or ML141 (*bottom*) and immunostained for filamin. Green arrowhead indicates enrichment of filamin at perinuclear region on soft ECM (*bottom*) post treatment with ML141. **e.** Line scan of normalized gray values of filamin along white dotted lines (**d**) shows perinuclear filamin enrichment peaks with ML141 treatment (bottom). **f.** MDCK-WT cells transfected with constitutively active Cdc42 ($Cdc42^{Q61L}$) and immunostained for filamin. Yellow arrowheads indicate increased interfacial enrichment of filamin on stiff ECM. Red arrowheads indicate enriched areas of constitutively active Cdc42. Scale bars, 10 μm.

Figure 4. Interaction with perinuclear cytoskeleton determines perinuclear filamin localization. a. Schematic representation for filamin structure, depicting its interactions with FAM101B and F-actin. The filamin-FAM101B-actin localization at perinuclear space is enabled by the complex's interaction with LINC complex, that responds to extracellular force cues. **b-e.** Immunofluorescence images of mApple-dnFLNA-MDCK (**b**), MDCK-mApple-dnFAM101B (**c**), mApple-dnNesprin1-MDCK (**d**) and mApple-dnLaminB1-MDCK (**e**) stained for filamin. White arrowheads indicate interfacial filamin localisation on stiff ECM. Green arrowheads (in ***b,c***) indicate finite perinuclear filamin localization only in a few mApple-dnFLNA or mApple-dnFAM101B cells. Scale bars: 10 μm. **f.** Box-and-whiskers plot depicting the fraction of filamin mean fluorescence intensity at perinuclear and interfacial regions, per cell, on stiff (90 kPa) ECM. Statistical significance was assessed using unpaired student t-test with Welch's correction (two-tailed). **g.** Schematic illustrating the tug-of-war model for dynamic localization of filamin, being pulled either towards the interfacial sink on soft ECM or towards the perinuclear sink on stiff ECM.

Figure 5. Rescuing EDAC on stiff ECM. **a.** An illustration showing the experimental design for rescuing EDAC on stiff ECM and the effect of different mosaic populations on extrusion of transformed cells on stiff ECM. **b-e.** Scatter bar plots depicting the fraction of GFP-$HRas^{V12}$ expressing colonies extruded over substrates of varying stiffness. For each stiffness, left bars are for mock MDCK-WT: MDCK-$HRas^{V12}$GFP and right bars are for mApple-dnFLNA-MDCK:MDCK-GFP-$HRas^{V12}$ (**b**), MDCK-mApple-dnFAM101B:MDCK-GFP-$HRas^{V12}$ (**c**), mApple-dnNesprin1-MDCK:MDCK-GFP-$HRas^{V12}$ (**d**) or mApple-dnLaminB1-MDCK:MDCK-GFP-$HRas^{V12}$ (**e**) mosaic populations. Stable expression of dnFLNA, dnFAM101B, dnNesprin1 or dnLaminB1 in surrounding cells rescued extrusion of transformed populations on stiff substrate. Data are mean±s.e.m. collected over 3 independent biological replicates. Statistical significance was assessed using Unpaired t-test with Welch's correction (two-tailed). The number of colonies counted is indicated inside each bar. **f.** Summary of the integrative mechanism that connects the processes occurring at different length-scales. We elucidate matrix mechanics, a microenvironmental factor (*panel A*), influences the molecular dynamics of filamin (*panels B and C*) to determine the outcome of EDAC (*panel D*).

Figures

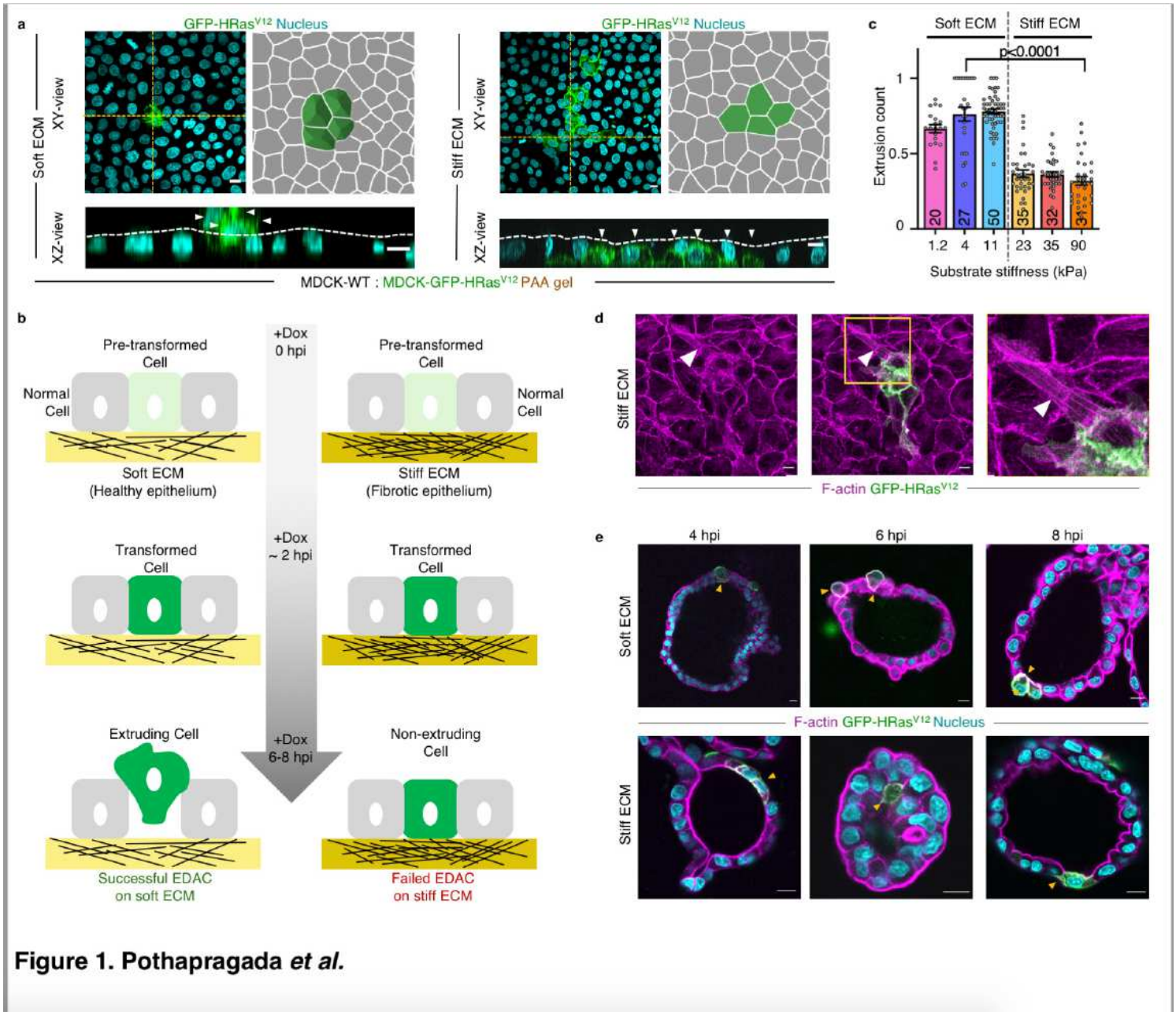

Figure 1. Pothapragada *et al.*

Figure 1

Matrix stiffening attenuates extrusion of HRasV12-transformed cells during EDAC. a. Fluorescence images of GFP-HRasV12 expressing colony extrusion on soft (4 kPa) and stiff (90 kPa) substrates in XY-plane; followed by an illustration depicting the visual metric employed to quantify extrusion. Rounded-up cells expressing GFP-HRasV12 (as seen on soft ECM) are taken as extruded. Non-extruded GFP-HRasV12 cells remain in plane with other cells, as evident on stiff ECM. (Bottom panels) The yellow-dotted lines visually guide epithelium surface in XZ-plane. GFP-HRasV12 cells extruded over this surface on soft ECM (left) whereas they remained within this surface on stiff ECM (right). White 1 arrowheads indicate GFP2-HRasV12 cells. b. Diagram representating different phases of extrusion of transformed cells and

stiffness-dependent outcome of EDAC. c. Scatter bar plot depicting the fraction of GFP-HRasV12 expressing colonies extruded over substrates of varying stiffness at 6 hpi. Distinct decrease in extrusion of transformed cells observed with increase in substrate stiffness. The number of colonies counted is indicated inside each bar. Data are mean±s.e.m. collected over 3 independent biological replicates. Statistical significance was assessed using Mann-Whitney t-test (two-tailed). d. Cytoskeletal morphology of non-extruded colonies over stiff ECM at 24 hpi. White arrowheads indicate basal actin fibres associated with HRasV12- cells on stiff ECM (90 kPa), stained with AlexaFluor647-Phalloidin. Inset: Magnified view of yellow-boxed region with actin fibres pointed out by white arrowheads. e. Immunofluorescence images of 3D cyst model for EDAC on soft and stiff ECM. Yellow arrowheads indicate the transformed cells. hpi: hours post-induction with doxycycline. a,d,e Scale bars: 10 μm.

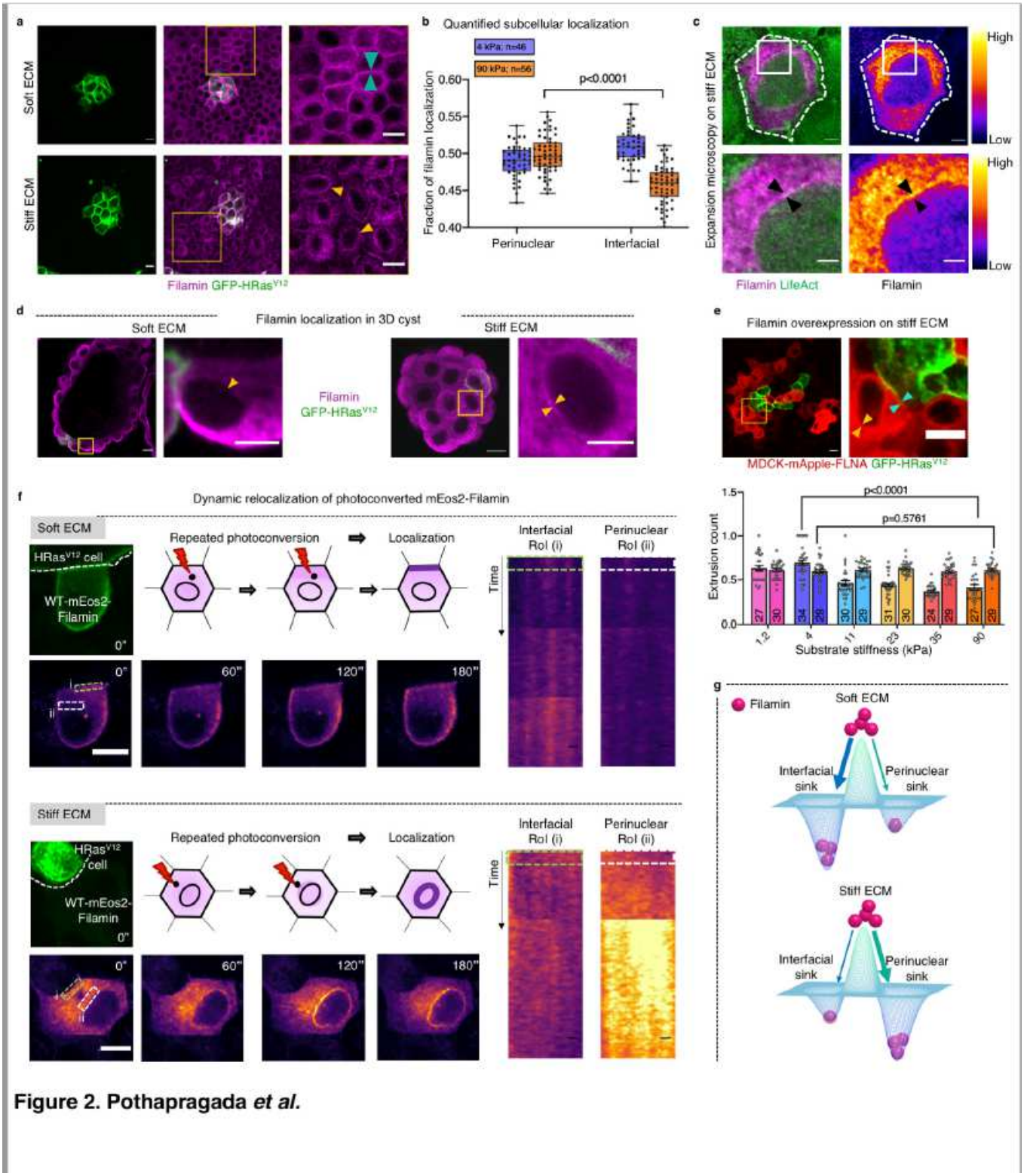

Figure 2. Pothapragada *et al.*

Figure 2

ECM stiffness-dependent localization of filamin determines EDAC efficacy. a. Immunostaining images of mosaic monolayer of MDCK-WT:MDCK-GFP-HRasV12 cultured on soft (top panels) and stiff (bottom panels) ECM. From left to right: GFP-HRasV12, filamin in the mosaic monolayer and magnified view of the boxed regions. Cyan arrowheads indicate interfacial filamin enrichment on soft ECM, and tellow arrowheads indicate perinuclear filamin localization on stiff ECM. Scale bars: 10 μm. b. Box-and-whiskers

plot depicting the fraction of filamin mean fluorescence intensity at perinuclear and interfacial regions, per cell, on soft (4 kPa) and stiff (90 kPa) ECM. Statistical significance was assessed using unpaired student t-test with Welch's correction (two-tailed). c. Ultrastructure expansion microscopy (U-ExM) for MDCK-LifeAct cells immunostained for filamin show distinct perinuclear co-localization (black arrowhead, bottom magnified panels). Scale bar: 1 μm (top) and 2 μm (bottom). d. Immunofluorescence images of filamin immunostaining in 3d cysts on soft (left) and stiff ECM (right) followed by the magnified view of boxed region. Presence or absence of filamin perinuclear localization indicated by yellow arrowheads for soft (absence) and stiff (presence) within MDCK-WT cells surrounding MDCK-GFP-HRasV12 cells. e. Fluorescence images of mosaic monolayer of filamin-over expressing MDCK cells and MDCK-GFP-HRasV12 co-cultured on stiff substrate with magnified view of the boxed region. Yellow and cyan arrowheads indicate perinuclear and interfacial filamin accumulation respectively. (Bottom) Scatter bar plot depicting the fraction of GFP-HRasV12 expressing colonies extruded over substrates of varying stiffness. For each stiffness, left bars are for mock MDCK-WT:MDCK-GFP-HRasV12 and right bars are for MDCK-mApple-FLNA:MDCK-GFP-HRasV12 mosaic populations. Stable over-expression of filamin in surrounding cells rescued extrusion of transformed populations on stiff substrate. f. Photoconversion of mEos2-filamin to study filamin localization dynamics. mEos2-filamin cell interfacing with an HRasV12 cell was stimulated and tracked for 180 seconds, as depicted in the schematic. Snapshots of mEos2-filamin dynamics indicating dynamic changes in localization. Kymographs of interfacial (i, green box) or perinuclear (ii, white box) regions show enrichment of filamin at interface (soft ECM, top panel) or perinuclear region (stiff ECM, bottom panel). Scale bars: 5 μm. g. Filamin attracting sinks. Filamin molecules can be imagined as the balls rolling downhill in the energy landscape to two competing attractor energy sinks, located at the cell-cell interface (left) and at the perinuclear region (right). On soft ECM, interfacial sink is deeper than perinuclear sink. Therefore, it attracts more filamin molecules than towards perinuclear. The scenario reverses on stiff ECM.

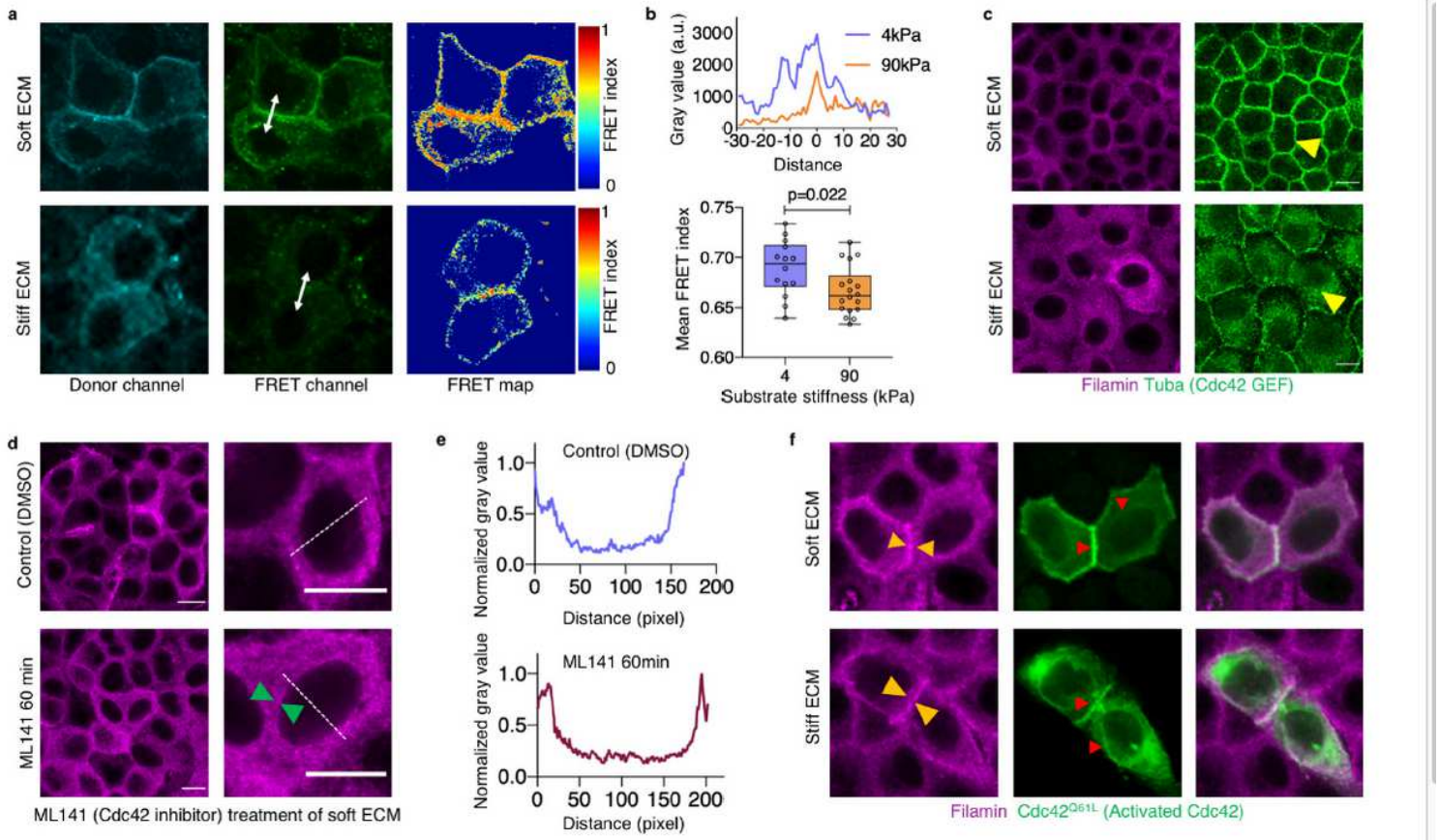

Figure 3. Pothapragada *et al.*

Figure 3

Interaction with Cdc42 determines interfacial filamin localization. a. Raichu- Cdc42 FRET biosensor expressed in MDCK-WT cells cultured on soft (top) and stiff (bottom) ECM. b. (Top) Line scan of normalized gray values from the FRET channel (white double-arrowed line in (a) from cells cultured on both soft and stiff ECM indicate higher FRET values at cell-cell interface on soft ECM. (Bottom) Box-and-whiskers plot of mean FRET index from soft and stiff ECM shows significant reduction in cells cultured on stiff ECM, indicative of higher Cdc42 activity on soft ECM. c. Immunofluorescence images of MDCK-WT cells co-stained for filamin and Tuba (Cdc42-GEF). Yellow arrowhead indicates enrichment of Cdc42-GEF at interfacial region on soft ECM (top) and at perinuclear region on stiff ECM (bottom). d. Immunofluorescence images of MDCK-WT cells cultured on soft ECM treated with Cdc42 inhibitor, control DMSO (top) or ML141 (bottom) and immunostained for filamin. Green arrowhead indicates enrichment of filamin at perinuclear region on soft ECM (bottom) post treatment with ML141. e. Line scan of normalized gray values of filamin along white dotted lines (d) shows perinuclear filamin enrichment peaks with ML141 treatment (bottom). f. MDCK-WT cells transfected with constitutively active Cdc42 (Cdc42Q61L) and immunostained for filamin. Yellow arrowheads indicate increased interfacial

enrichment of filamin on stiff ECM. Red arrowheads indicate enriched areas of constitutively active Cdc42. Scale bars, 10 μm.

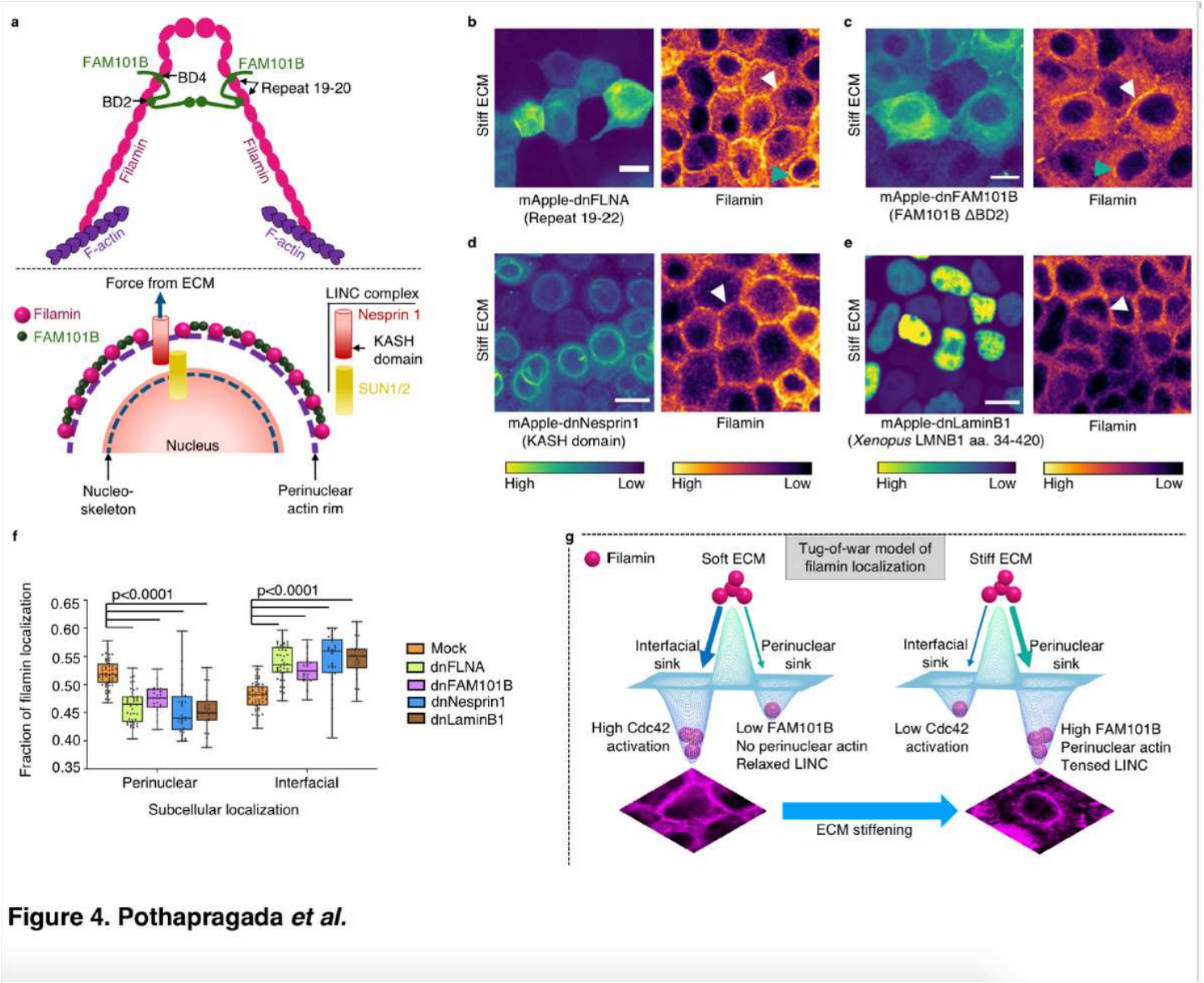

Figure 4. Pothapragada *et al.*

Figure 4

Interaction with perinuclear cytoskeleton determines perinuclear filamin localization. a. Schematic representation for filamin structure, depicting its interactions with FAM101B and F-actin. The filamin-FAM101B-actin localization at perinuclear space is enabled by the complex's interaction with LINC complex, that responds to extracellular force cues. b-e. Immunofluorescence images of mApple-dnFLNA-MDCK (b), MDCK-mApple-dnFAM101B (c), mApple-dnNesprin1-MDCK (d) and mApple-dnLaminB1-MDCK (e) stained for filamin. White arrowheads indicate interfacial filamin localisation on stiff ECM. Green arrowheads (in b,c) indicate finite perinuclear filamin localization only in a few mApple-dnFLNA or mApple-dnFAM101B cells. Scale bars: 10 μm. f. Box-and-whiskers plot depicting the fraction of filamin mean fluorescence intensity at perinuclear and interfacial regions, per cell, on stiff (90 kPa) ECM. Statistical significance was assessed using unpaired student t-test with Welch's correction (two-tailed). g.

Schematic illustrating the tug-of-war model for dynamic localization of filamin, being pulled either towards the interfacial sink on soft ECM or towards the perinuclear sink on stiff ECM.

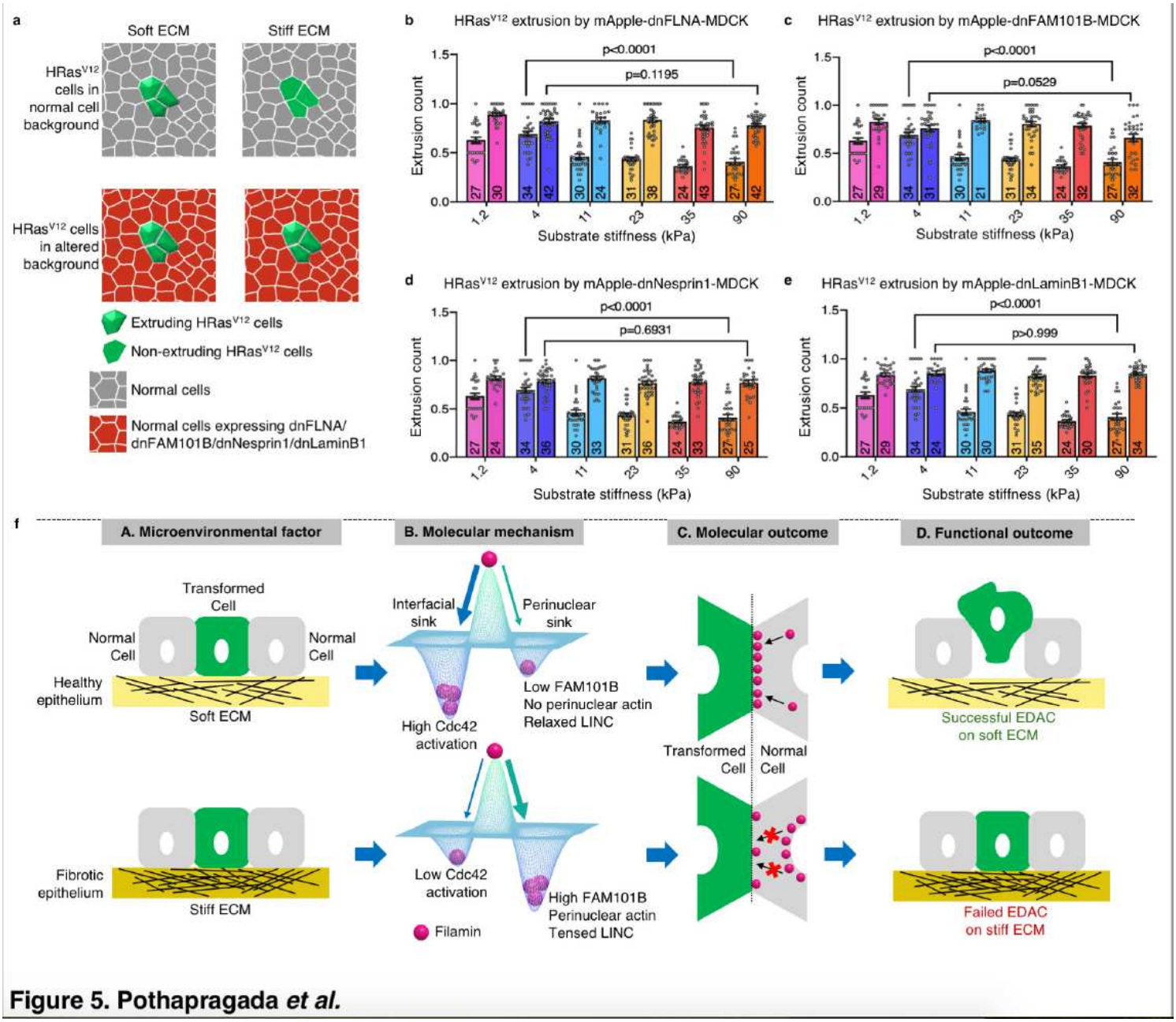

Figure 5. Pothapragada *et al.*

Figure 5

Rescuing EDAC on stiff ECM. a. An illustration showing the experimental design for rescuing EDAC on stiff ECM and the effect of different mosaic populations on extrusion of transformed cells on stiff ECM. b-e. Scatter bar plots depicting the fraction of GFP-HRasV12 expressing colonies extruded over substrates of varying stiffness. For each stiffness, left bars are for mock MDCK-WT: MDCK-HRasV12GFP and right bars are for mApple-dnFLNA-MDCK:MDCK-GFP-HRasV12 (b), MDCK-mApple-dnFAM101B:MDCK-GFP-HRasV12 (c), mApple-dnNesprin1-MDCK:MDCK-GFP-HRasV12 (d) or mApple-dnLaminB1- MDCK:MDCK-GFP-HRasV12 (e) mosaic populations. Stable expression of dnFLNA, dnFAM101B, dnNesprin1 or dnLaminB1 in surrounding cells rescued extrusion of transformed populations on stiff substrate. Data

are mean±s.e.m. collected over 3 independent biological replicates. Statistical significance was assessed using Unpaired t-test with Welch's correction (two-tailed). The number of colonies counted is indicated inside each bar. f. Summary of the integrative mechanism that connects the processes occurring at different length-scales. We elucidate matrix mechanics, a microenvironmental factor (panel A), influences the molecular dynamics of filamin (panels B and C) to determine the outcome of EDAC (panel D).

Supplementary Files

This is a list of supplementary files associated with this preprint. Click to download.

- SupplementaryVideo1.avi
- SupplementaryVideo2.avi
- SupplementaryVideo3.avi
- SupplementaryInformation.pdf